

Influence of interaction softness in phase separation of active particles

Monika Sanoria,¹ Raghunath Chelakkot,^{1,*} and Amitabha Nandi^{1,†}

¹*Department of Physics, Indian Institute of Technology Bombay, Powai, Mumbai, 400076, India.*

Using a minimal model of active Brownian discs, we study the effect of a crucial parameter, namely the softness of the inter-particle repulsion, on motility-induced phase separation. We show that an increase in particle softness reduces the ability of the system to phase-separate and the system exhibit a delayed transition. After phase separation, the system state properties can be explained by a single relevant lengthscale, the effective inter-particle distance. We estimate this lengthscale analytically and use it to rescale the state properties at dense phase for systems with different interaction softness. Using this lengthscale, we provide a scaling relation for the time taken to phase separate which shows a high sensitivity to the interaction softness.

I. INTRODUCTION

The last two decades witnessed a growing interest in the study of *active matter* [1–3], a system microscopically composed of a collection of motile entities that drive the system out-of-equilibrium. The collective behaviour of such active systems has been studied using particle-based numerical models where individual active agents self-propel along a body-fixed polarity vector. The large-scale collective behaviour crucially depends on the mutual interaction. One well-studied class of models involves interaction between the particles via a pairwise potential, affecting only their positions. For such a system, the interplay between activity and repulsion leads to phase separation, forming a dense phase and a dilute phase. This is commonly known as motility induced phase separation (MIPS) [4–9]. Unlike equilibrium phase transition, MIPS occurs in the absence of any attractive interaction [9–26].

While the physical principles governing MIPS has been extensively studied before [25, 27, 28], a crucial question that remains is how sensitive are they to the softness or deformability of the microscopic entities. The dependence of two-phase coexistence on interaction softness has been observed in passive systems [29]. To model active colloidal particles that are *practically* non-overlapping, the Weeks-Chandler-Anderson (WCA) form has been used extensively [30]. Recent studies have also explored the hard particle limit by reducing the overlap beyond WCA and characterized the complete phase behavior [10]. Another interesting limit is to study how an increase in the mutual overlap between the particles affect the collective properties of the system. This limit is relevant from the perspective of microscopic biological entities, such as cells in tissues. Since they are deformable objects, hard potentials may not be a proper representation of the interaction between them. Furthermore, the mechanical properties of the individual entities may vary during the course of development [31] which can affect their collective properties. To understand how such

a variation in the interaction affects the structural, dynamic, and phase properties, we use a minimal model of active Brownian particles and study their collective behaviour by systematically varying the interaction softness. We show that the change in phase behaviour with varying softness can be rescaled by an intrinsic lengthscale, which is the effective inter-particle distance. In the following sections, we discuss the model and the numerical techniques, followed by the results and a discussion of the results.

II. MODEL

Our numerical model consists of a collection of N active Brownian particles in 2D that interact with their neighbors repulsively. The repulsive force between the particles at locations \mathbf{r}_i and \mathbf{r}_j due to excluded volume interaction is obtained from the generalized WCA potential [32],

$$u(r) = \varepsilon^{-1} V_{ex} = \begin{cases} 4 \left[\left(\frac{\sigma}{r} \right)^{2\alpha} - \left(\frac{\sigma}{r} \right)^\alpha \right] + 1 & ; r/\sigma < 2^{1/\alpha} \\ 0 & ; r/\sigma > 2^{1/\alpha}, \end{cases} \quad (1)$$

where $r = |\mathbf{r}_i - \mathbf{r}_j|$, σ is the nominal particle diameter, and the characteristic energy of the system is chosen to be $\beta^{-1} = k_B T$. Here α is the parameter that controls the particle stiffness; lower α denotes soft interaction limit with larger area overlap while upon increasing α , the particles become harder and overlap less. The equation of motion of each active particle in non-dimensionalized units is described by the coupled Langevin equations in the overdamped limit (see Appendix A)

$$\dot{\mathbf{r}}_i = -\nabla_i u + \text{Pe} \hat{\mathbf{n}}_i + \xi_i, \quad (2)$$

$$\dot{\theta}_i = \xi_i^R. \quad (3)$$

Here, ξ_i and ξ_i^R are the Gaussian white noise terms with zero mean and satisfy $\langle \xi_i(t) \xi_j(t') \rangle = 2\delta_{ij} \delta(t - t')$, and $\langle \xi_i^R(t) \xi_j^R(t') \rangle = 6\delta_{ij} \delta(t - t')$. The direction of self-propulsion for each particle is $\hat{\mathbf{n}}_i = (\cos \theta_i, \sin \theta_i)$. Our minimal model has three relevant control parameters: density ϕ , the Péclet number Pe , which quantifies the activity strength and the overlap parameter, α .

* raghu@phy.iitb.ac.in

† amitabha@phy.iitb.ac.in

Using Eqs. (2–3), we performed Brownian dynamics simulations using an Euler integration step inside a periodic square-box (see Appendix A).

III. RESULTS

We first study the effect of α on density order. We benchmark our numerical study to the WCA case ($\alpha = 6$), where the system exhibits a very clear phase separation [5]. We aim to quantify any deviation from the known results as α is decreased below 6. To characterize this, we compute the local density ϕ_{loc} . For a single uniform phase, the density distribution $P(\phi_{loc})$ is unimodal while for the phase-separated system $P(\phi_{loc})$ is bi-modal. We denote the peak values of the dense and dilute phases as ϕ_l and ϕ_g , respectively. In Fig. 1, we

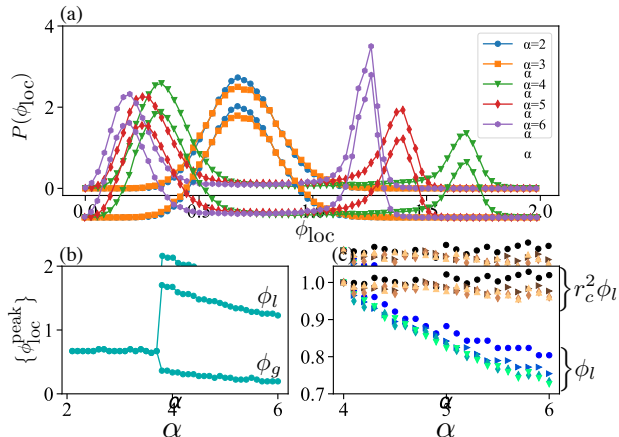


FIG. 1. (a) Comparison of the local density distribution $P(\phi_{loc})$ at $\phi = 0.7$ and $Pe = 150$ for different α values. (b) The peak value of the $P(\phi_{loc})$ distributions observed in (a) are plotted as a function of α . The bifurcation indicates the appearance of the dense phase as α is increased. (c) Scaling of the dense phase density ϕ_l with α is plotted for $Pe = 100$ (\bullet), 130 (\blacklozenge), 150 (\blacklozenge), and 170 (\blacktriangledown), for $\phi = 0.7$. For convenience the ϕ_l has been normalized by $\phi_l(\alpha = 4)$. For $\phi_l \rightarrow r_c^2 \phi_l$, the α dependence disappears.

compare $P(\phi_{loc})$ for different α at $\phi = 0.7$ and $Pe = 150$. We notice that the phase separation is still observed for $\alpha < 6$ (see Fig. 1(a), for $\alpha = 5$ and 4). As we decrease α even further, we do not see a clear phase separation even when the activity is made very high (see Fig. 6, for $Pe = 300$ at $\alpha = 3$ and $\phi = 0.7$), except for a very large density ($\phi \simeq 0.98$ and $Pe \gtrsim 150$) (see Fig. 7). Such a high density is only accessible for particles with large area overlap and we do not make a detailed comparative study here. Interestingly, we also note that as α is reduced, there is an overall decrease in the area covered by the dense phase (see Fig. 5(b)–(d) in Appendix. A and Fig. 8 in Appendix. B). To identify phase transition, we plot the corresponding peak values of $P(\phi_{loc})$ as a function of α (see Fig. 1(b)). We observe, the creation of two

distinct phases ϕ_l and ϕ_g for $\alpha \approx 3.7$. Similar disappearance of coexistence with increasing particle softness has been observed earlier in 2D equilibrium systems as well for an inverse power-law pair interaction [29].

After phase separation, there is a systematic shift in ϕ_l , and ϕ_g to lower values, as α is increased. In Fig. 1(c), we have plotted ϕ_l as a function of α for different values of Pe at $\phi = 0.7$, which clearly shows this monotonic decrease. This is due to the fact that a smaller α leads to a decrease in the average inter-particle distance causing an increase in density. To explain this increase in ϕ_l for lower α , we use a mean-field description proposed earlier [27]. Within this framework the density dependent effective speed is given by $v(\rho) \equiv Pe - \rho\zeta$, where ρ is the number density and ζ quantifies the local force-balance in the system and is given by $\zeta = \int_0^\infty r[-\nabla u(r)]K(r)dr$, where $u(r)$ is the effective pair interaction and $K(r) = \int_0^{2\pi} \cos\theta g(r, \theta)d\theta$, where $g(r, \theta)$ is the stationary pair-distribution function. For a single homogeneous phase, and for a given α , $\rho(\mathbf{r}, t) = \bar{\rho}$ is constant. To estimate the effective cut-off distance r_c between the particles, we consider the scenario where the dense phase has already been formed and we write $\zeta \approx \int_{r_c}^\infty r[-\nabla u(r)]K(r)dr$. Furthermore, within the dense phase $v(\bar{\rho}) \ll Pe$, we therefore set $v(\bar{\rho}) \approx 0$. Note that a systematic estimate of r_c would involve an estimation of $g(r, \theta)$ (and hence $K(r)$) from simulation data, for different α . Here we make a simplifying assumption $K(r) \approx K\delta(r - r_c)$, since the dense phase has a crystalline structure where $K(r)$ shows the first peak around $r \simeq r_c$. This leads to:

$$r_c \approx 4^{1/\alpha} \left(1 + \sqrt{1 + \frac{2Pe}{\alpha C}} \right)^{-1/\alpha}. \quad (4)$$

Here $C = \bar{\rho}K$, which in general depends on α . Eq. 4 can be used to estimate r_c if C is known. As a first approximation we assume C to be a constant [33]. To see if this could justify the behavior of ϕ_l , we estimate r_c using Eq. 4 and using C as a fit parameter. We rescale $\phi_l \rightarrow r_c^2 \phi_l$. For $C \approx 0.45$, we notice that the dependence on α disappears as $r_c^2 \phi_l$ is approximately a constant (see Fig. 1(c)).

We also note in Fig. 1(a)) that with increasing α , the distribution of the dense phase about ϕ_l becomes narrower, indicating a larger uniformity within the dense phase at higher α . Finally, we note that although for $\alpha \lesssim 3.7$ we do not observe a phase coexistence (see Fig. 1(b)), the overall phase properties at large Pe are different from a homogeneous phase typically observed at low Pe . Here the system exhibits a complex spatiotemporal dynamics, where we observe a large number of small local clusters that are not stable over time (see Fig. 5(d) in Appendix A and Movie 1 in [34] for $\alpha = 3$ and $Pe = 150$).

The appearance of dense phase and its dependence on α can be understood by quantifying the pressure in presence of activity [35–40]. We calculate the normalized

pressure $\tilde{P} = P\phi/P_{id}$, where P is the total pressure, calculated by combining the contributions from both thermal fluctuations and activity [39] for the our system (See Eq. C1 in Appendix C), and $P_{id} = \frac{N}{A}(1 + \frac{Pe^2}{6})$ [39]. Here A is the total area in non-dimensional units. In Fig. 2 we show \tilde{P} for $\alpha = 6$ (Fig. 2(a)) and 3 (Fig. 2(b)) as a function of ϕ and Pe . At $\alpha = 6$, we observe a drop in the value of \tilde{P} in the ϕ - Pe parameter space where the system phase separates. For $\alpha = 3$, the phase separation is shifted to a large value of ϕ and Pe . This is visible in Fig. 2(b) — we observe a small region in ϕ - Pe parameter space where \tilde{P} drops to a smaller value. For a given Pe , the α dependence of the normalized pressure \tilde{P} is summarized in Fig 2(c). We see how, with decreasing α , the critical density ϕ_{cr} , shift to higher densities until it disappears. This systematic shift of the critical point, can be explained as the following: we note that for all $\phi > \phi_{cr}$, $\phi = (N_l + N_g)\pi/A$, where N_l and N_g are the number of particles in the dense and dilute phases. Based on the numerical evidence (see Fig.9 in Appendix. D), we assume $\phi_g \approx f_\alpha \phi_l$, where $f_\alpha < 1$ is a scale-factor with a weak dependence on α . This leads to $\phi \approx \phi_l h(\alpha)$, where $h(\alpha)$ is an unknown function that explicitly depends on the area occupied by the dilute phase (see Appendix D). Making a simplifying assumption that $h(\alpha)$ have a power-law dependence on α , we scale the ϕ -axis, i.e. $\phi \rightarrow r_c^2 \alpha^\gamma \phi$ for different α values where phase separation has been observed. Using the r_c value calculated previously using Eq. 4, and for $\gamma \approx 0.17$, we are able to collapse the transition points along the ϕ -axis indicating that the critical density ϕ_{cr} also follows the same scaling (see Fig. 2(d)). The small value of the exponent γ is consistent with our prediction that $h(\alpha)$ is weakly dependent on α (see Appendix D). The bulk pressure in the dense phase also follows a similar scaling, i.e. $\tilde{P} \rightarrow r_c^2 \alpha^\delta \tilde{P}$ with $\delta \approx 0.45$ (Fig. 2(d)), implying the qualitatively same α dependence as seen for the case of ϕ . Note that before phase separation, \tilde{P} can be rescaled by the Boltzmann diameter $r_B = 2^{1/\alpha}(1 + \sqrt{g_{\alpha,\phi}})^{-1/\alpha}$ derived from equilibrium considerations [32]. Here $g_{\alpha,\phi}$ is a collision parameter that depends on both the softness and the density. We estimate $g_{\alpha,\phi}$ from [32] (see Appendix E) and rescale $\tilde{P} \rightarrow r_B^2 \tilde{P}$. As shown in the inset of Fig. 2(d), the curves collapse reasonably well, especially at low ϕ values, as expected.

Having looked into the dependence of density ordering and the bulk pressure on the overlap parameter α , we now study how the structural properties of the system is affected by changing this parameter. For this purpose we study the global orientational order, $\psi_6 = \left\langle \left| \frac{1}{N} \sum_{i=1}^N \phi_{6i} \right| \right\rangle$, where $\phi_{6i} = \frac{1}{N_b} \sum_{j \in N_b} e^{6i\theta_{ij}}$, calculated at the location of every particle i . Here N_b is the total number of neighbours of the i^{th} particle obtained using Voronoi tessellation, θ_{ij} is the angle between the vector \mathbf{r}_{ij} and the reference axis.

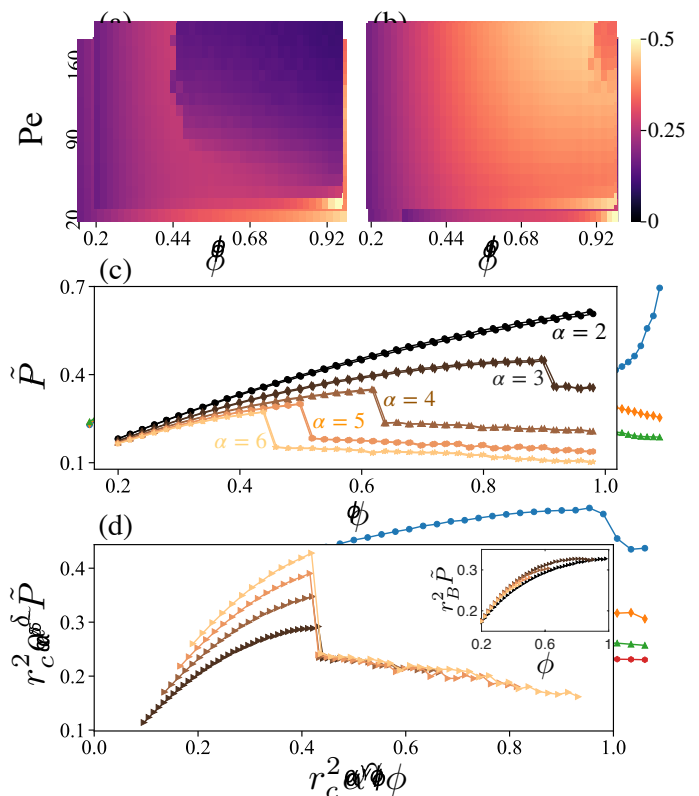


FIG. 2. Study of the normalized pressure $\tilde{P} = P\phi/P_{id}$. (a) and (b) shows the heat maps of \tilde{P} in the Pe - ϕ plane for $\alpha = 6$ and $\alpha = 3$ respectively. (c) \tilde{P} plotted as a function of ϕ at $Pe=150$ for $\alpha = 2 \rightarrow 6$. (d) Study of scaling behavior for the phase separating cases shown in (c). The ϕ -axis is scaled by, i.e. $r_c^2 \alpha^\gamma$, with $\gamma \approx 0.17$, while the pressure-axis is scaled with a factor $r_c^2 \alpha^\delta$ ($\delta \approx 0.45$). The inset show the scaling of \tilde{P} before phase separation, using the Boltzmann diameter r_B .

In Fig. 3(a)–(c) we compare the ψ_6 heatmaps in the ϕ - Pe plane for $\alpha = 6, 4$, and 3. We notice that the phase separated domain, indicated by a large ψ_6 ($\gtrsim 0.4$) value, gradually decreases in size in the ϕ - Pe plane as α is varied from 6 \rightarrow 3. Furthermore, the phase boundary (defined by $\psi_6 \approx 0.4$) also gradually shifts towards higher values of Pe and ϕ , as α is decreased. There is also an increase in the sixfold symmetry within the dense phase for larger α , due to an increase in the cluster size (see Fig.8 in Appendix. B). This behaviour is consistent with our observation of the local density distributions shown in Fig. 1 for $\phi = 0.7$. Using the same scaling relation for ϕ_{cr} in the pressure analysis (Fig 2(d)), we rescaled $\phi \rightarrow r_c^2 \alpha^\gamma \phi$, which leads to a collapse of ϕ_{cr} for different α (See Fig.10(b) in Appendix. F). We also note that $\psi_6 \sim r_c$ after phase separation (See Fig.10(b)).

We also note for $\alpha = 6$, at low Pe and large ϕ , there is an enhanced global order (see Fig. 3(a)). Such behavior has also been observed recently in systems of active Brownian particles, even with lesser overlap [10]. This feature is not seen for $\alpha = 4$ and 3 (Fig. 3(e)–(f)) since the larger overlap between the particles destroys the hex-

atic order at such high densities.

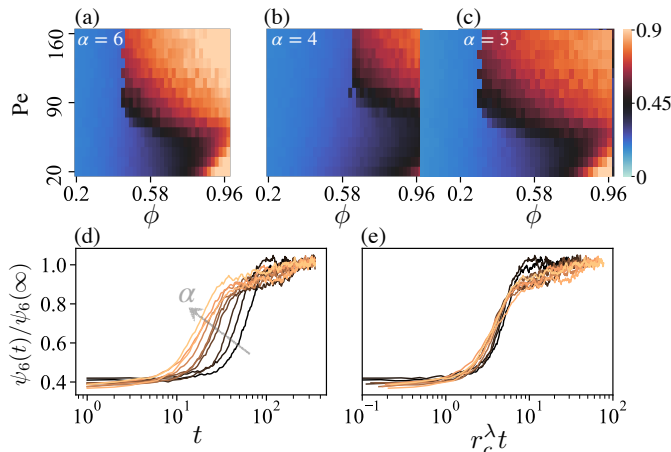


FIG. 3. Quantification of global orientational order. (a)–(c) The global orientational order parameter ψ_6 is shown as a colormap in the ϕ – Pe plane. Dynamics of phase-separation as a function of α . (d) $\psi_6(t)/\psi_6(\infty)$ ($\psi_6(\infty)$ is the steady state value) plotted as a function of time for $\alpha = 4 \rightarrow 6$ with $\Delta\alpha = 0.2$. Here $Pe=150$ and $\phi = 0.7$. (e) Demonstration of temporal scaling. Introducing a scaling $t \rightarrow r_c^\lambda t$, leads to a collapse of all the different plots for $\lambda \approx 8.5$.

To understand how the emergence of phase ordering changes with varying α , we plot $\psi_6(t)$ versus time starting from a homogeneous phase for different values of α . While a more detailed approach to address this question will involve the study of coarsening dynamics, the ψ_6 dynamics can also be used to investigate this transition. In Fig. 3(d), we plot $\frac{\psi_6(t)}{\psi_6(\infty)}$ as a function of time, where $\psi_6(\infty)$ is the steady-state value after the system has already phase-separated. We notice that with a decrease in α , the system takes longer to phase-separate. To quantify this dependence on particle softness, we apply a rescaling of the time axis, $t \rightarrow r_c^\lambda t$. We use r_c instead of α for rescaling (see Fig.11(b) in Appendix. F), since it is an intrinsic length-scale, which can be obtained in general for any form of the potential used. This rescaling leads to a data collapse for $\lambda \approx 8.5$ (see Fig. 3(e)). The large value of λ indicative of sensitive dependence of the transition time on α . This dependence can also be of an exponential form (see Fig.11(c) in Appendix. F).

Our study so far has revealed the dependence of the static quantities, such as ϕ_{cr} , ϕ_l , \tilde{P} , and ψ_6 on α , in a phase-separated system, through a system lengthscale, r_c , defined for the dense-phase. Also, it shows that the time required for the system to phase separate is sensitive to α . A natural question arises whether the transport properties within the dense-phase also vary with α . To study this, we compute the mean-square displacement (MSD) of one or a few tagged particles inside the dense phase. In Fig. 4, we show the MSD of a tag-particle, inside the dense phase, as a function of lag-time (t) for $4.0 \leq \alpha \leq 6$, $Pe=150$, and $\phi = 0.7$. We note that the

MSD for $\alpha = 6$ shows good agreement with the reported results [5]. Interestingly, the MSD behaviour did not show any noticeable change as α is varied. This indicates that once the system phase-separates, unlike the static quantities, the particle dynamics is almost independent of α . This observation is further strengthened by the MSD behaviour for $\alpha = 3$ and 2 at $\phi = 0.7$ and $Pe=150$, where there is no single large cluster but the formation of many small local dynamic clusters. In this case, for the same values of ϕ and Pe , we notice a deviation in the MSD behaviour (see Fig. 4(b)), qualitatively different from the previous observations in both the dilute phase and dense phase (see Fig.12 in Appendix. G), indicating a different collective dynamics which needs to be studied in detail.

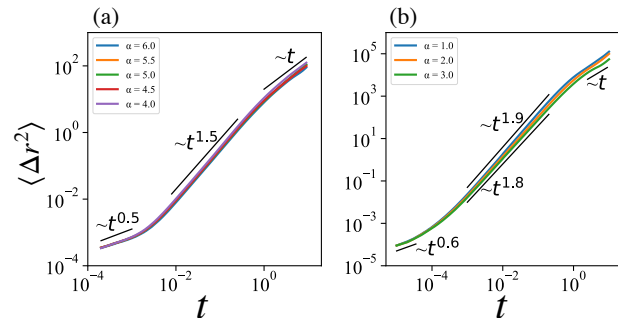


FIG. 4. (a) Mean-square displacement $\langle \Delta r^2(t) \rangle$ of a particle inside the dense phase for different α . (b) $\langle \Delta r^2(t) \rangle$ plotted for $\alpha = 3$ in the case when the system does not phase separate to form a single large cluster. Here $Pe=150$ and $\phi = 0.7$.

IV. CONCLUSION

Our study reveals that an increase in interaction softness has an inhibiting effect on phase separation and strongly influences the collective phase ordering: the critical density above which the system phase separates shifts to higher values, while the waiting time for observing a phase separation, above the critical density, also increases. The phase separation in the system is manifested by an intrinsic lengthscale, which is the effective inter-particle distance r_c . The changes in state properties with interaction softness in the dense phase can be explained using r_c . Using a mean-field theory [27], we make an approximate estimate of r_c which explain the α dependence of the dense phase reasonably well. Using a relation between the dense and dilute phase densities obtained numerically, we show that the critical density at the onset of phase ordering and the corresponding bulk pressure can be scaled using the same r_c with power-law corrections. Before the phase separation, the rescaling can be achieved reasonably by the Boltzmann diameter, r_B . To characterize the temporal efficiency as a function of α , we also studied the time evolution of the global hexatic order for different α . We found that an increase in par-

ticle softness (or decrease in α), significantly slows down the approach to transition and scales as $\sim r_c^{8.5}$. However, the transport properties within the dense phase show no variation with α . This indicates that once the system phase separates, the dynamic behaviour inside the dense phase is weakly dependant on the microscopic interaction parameters. Note that the disappearance of phase separation has been observed in inertial systems, with an increase in Pe to ε ratio [41, 42]. It would be interesting to explore, how an increase in interaction softness modify this behaviour.

The dependence of phase separation on interaction softness has relevance beyond simple models of active matter. The mutual interactions in many active biological systems are not hard-core in nature and may vary across systems. Our study thus may provide a physical basis for phase ordering in such systems. This behaviour need not be specific to the particular form of interaction we have used, and we expect to observe similar behaviour with other forms of short-ranged repulsive interactions.

ACKNOWLEDGEMENTS

The authors thank Debasish Chaudhuri, Dibyendu Das, and Mithun K. Mitra for insightful discussions. MS thank CSIR, India for financial support. AN and RC acknowledges Industrial Research and Consultancy Centre (IRCC) at IIT Bombay, India, and Science and Engineering Research Board (SERB), India (Project No. ECR/2016/001967, ECR/2017/000744, and SB/S2/RJN-051/2015) for financial support. We thank IIT Bombay HPC facility (Spacetime2).

Appendix A: Simulation Method

Our numerical model consists of a collection of active Brownian particles in 2D that interact with its neighbors repulsively. The repulsive force $\mathbf{F}_{ex}(\mathbf{r})$ between the particles at locations \mathbf{r}_i and \mathbf{r}_j due to excluded volume interaction is obtained from the generalized WCA potential [32] $V_{ex}(r)$ given in Eq. 1.

Each particle is represented by a position vector \mathbf{r}_i and moves with self-propelled constant speed v_p along a direction \mathbf{n}_i , where $\mathbf{n}_i = (\cos \theta_i, \sin \theta_i)$. The particle direction \mathbf{n}_i are evolved randomly in time and equation of motion of active particle is described by the coupled and over-damped Langevin equations

$$\dot{\mathbf{r}}_i = v_p \hat{\mathbf{n}}_i + \mu \mathbf{F}_{ex}(\mathbf{r}) + \boldsymbol{\xi}_i, \quad (\text{A1})$$

$$\dot{\theta}_i = \xi_i^R. \quad (\text{A2})$$

Eqs. (A1–A2) are non-dimensionalized to obtain Eqs. (2–3) using the particle diameter σ , thermal energy $\beta^{-1} = k_B T$ and relaxation time $\tau = \frac{\sigma^2}{D_t}$. The characteristic energy of the system is chosen to be $\varepsilon = \beta^{-1}$.

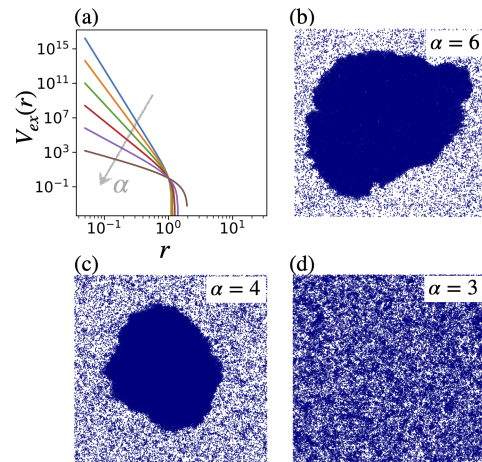


FIG. 5. Effect of the overlap parameter α on the phase behavior. (a) Interaction potential $V_{ex}(\mathbf{r}_{ij})$ plotted against r_{ij} for different values of α varied from $6 \rightarrow 1$. (b)–(d) shows the steady state snapshots indicating the phase behavior for a system of $N = 40,000$ particles, at $\phi = 0.7$, $Pe=150$.

Here, v_p is the active self propulsion speed of each particle and $\mu = \beta D_t$ is the mobility parameter, D_t is translational diffusion coefficient, and $D_r = 3D_t/\sigma^2$, is the rotational diffusion coefficient. $\boldsymbol{\xi}_i$ and ξ_i^R are the Gaussian white noise terms with mean zero and variance unity and satisfies $\langle \boldsymbol{\xi}_i(t) \boldsymbol{\xi}_j(t') \rangle = 2D_t \delta_{ij} \delta(t - t')$, and $\langle \xi_i^R(t) \xi_j^R(t') \rangle = 2D_r \delta(t - t')$.

The effect of activity is studied by varying the Péclet number (Pe), a non-dimensional parameter defined as $Pe = v_p \frac{\tau}{\sigma}$. Our minimal model has three relevant control parameters: density ϕ , activity strength Pe, and interaction parameter α . To characterize the system, these parameters are varied such that, $\phi \in [0.1, 0.98]$, $Pe \in [20, 180]$ and $\alpha \in [2, 6]$.

We performed Brownian dynamics simulations using Euler integration step inside a periodic square-box for $N = 40000$ to 112000 particles and with Brownian time step $\Delta t = 10^{-5} \tau$ upto $t = 100 \tau$. The translational diffusion coefficient is chosen to be $D_t = 1$ throughout.

Appendix B: Phase behavior for the case of $\alpha < 6$

Appendix C: Active pressure for 2D active system

Total pressure of a 2D active system with area A and total number of particles N , can be calculated using the following expression [39]

$$P = \frac{1}{A} \left\{ N + Pe \frac{Nv}{6} + \frac{1}{4} \sum_{i=1}^N \sum_{j=1}^N \sum_n \langle \mathbf{F}_{ij}^n \cdot (\mathbf{r}_i - \mathbf{r}_j - \mathbf{R}_{ij}^n) \rangle \right\}. \quad (\text{C1})$$

Here the first term on the right hand side is the thermal contribution and the second term is the swim pressure. Here, $v = \frac{1}{N} \sum_{i=1}^N \langle \dot{\mathbf{r}}_i \cdot \hat{\mathbf{n}}_i \rangle$ is defined as the mean speed

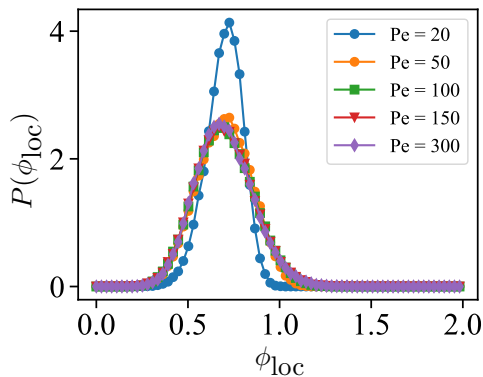


FIG. 6. Local density distribution $P(\phi_{loc})$ with varying Pe at $\phi = 0.7$ and $\alpha = 3$. We notice that the system does not phase separate even at large value of activity ($Pe=300$).

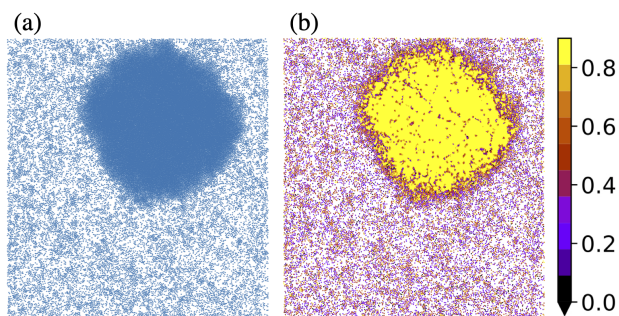


FIG. 7. (a) Phase separation observed for $\alpha = 3$ at very large densities ($\phi = 0.98$). Here we set $Pe=170$ and the simulation was run for a system of $N = 40,000$ particles. (b) shows the local orientational order ϕ_{6i} as a color coded value superimposed on particle configurations.

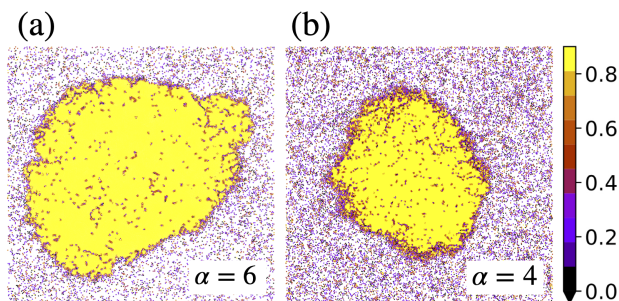


FIG. 8. Local orientational order ϕ_{6i} as a color coded value superimposed on particle configurations in the $x-y$ plane for different $\alpha = 6$ and 4 respectively. Here we set $\phi = 0.7$ and $Pe=150$. For $\alpha = 6$, we notice that there are few defect points of mainly 5-7 pairs present within the dense region (see (a)). Similar defect points are also observed in the dense phase for $\alpha = 4$ but the number is higher. This is possibly caused by the large overlap between the particles in this case causing deviations from the six-fold symmetry locally.

of the active particle. The last term is contribution due to inter-particle interaction. The last two terms in Eq. C1 is called the total active pressure.

Appendix D: Critical Density

Let ϕ_{cr} be the critical density at which phase separation occurs. We assume there are N_l number of particles in the dense (liquid) phase and N_g in the dilute (gas) phase. Let A_l and A_g be the area of the dense and dilute phases respectively. Therefore, ϕ_{cr} can be written as

$$\phi_{cr} = \frac{N_l + N_g}{A} = \phi_l \frac{A_l}{A} + \phi_g \frac{A_g}{A}. \quad (D1)$$

By comparing the values of ϕ_l and ϕ_g obtained numer-

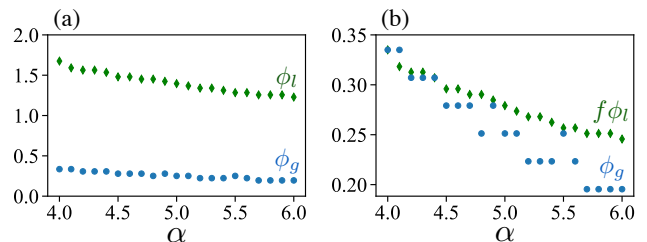


FIG. 9. (a) Values of ϕ_l (\blacklozenge) and ϕ_g (\bullet) plotted as a function of α at $\phi = 0.7$ and $Pe=150$. (b) To compare the trend we multiply ϕ_l by a factor of $f = 0.2$.

ically (see Fig. 9), we note that both shows a similar dependence on α and we can assume $\phi_g \approx f_\alpha \phi_l$. Here f_α is weakly dependent on α with magnitude < 1 . Substituting this in Eq. D1, we obtain

$$\phi_{cr} \approx \phi_l \left[1 - (1 - f_\alpha) \frac{A_g}{A} \right] \approx \phi_l h(\alpha) \quad (D2)$$

Here $(1 - f_\alpha) < 1$ and weakly dependent on α and $\frac{A_g}{A}$ is also a function of α with magnitude less than unity. Therefore the quantity $h(\alpha)$ is expected to have a weak dependence on α as well.

Appendix E: Scaling using the Boltzmann diameter

Taking the collision energy to be of the order of $K_B T$, one can derive the typical interparticle distance, namely the Boltzmann parameter given by [32]

$$r_B = \left(\frac{2}{1 + \sqrt{g_{\alpha,\phi}}} \right)^{1/\alpha} \quad (E1)$$

Here $g_{\alpha,\phi}$ is a collision parameter and depends on both the α and ϕ . We assume a functional form for the collision parameter $g_{\alpha,\phi} \sim \alpha^{a_1} \phi^{a_2}$ where a_1 and a_2 are constant exponents. Using the simulation data reported in Ref. [32] (Table-I), we obtain $a_1 \approx -0.74$, and $a_2 \approx 1.12$. The estimated values of r_B using a form of $g_{\alpha,\phi} \approx 12.54 \alpha^{-0.74} \phi^{1.12}$ leads to a reasonably good scaling of \tilde{P} (shown in the inset of Fig. 2(d)) before phase separation.

Appendix F: Hexatic order parameter scaling

Similar to the \tilde{P} versus ϕ plot shown in Fig. 3(c), ψ_6 also shows a sharp change in value at a critical density value ϕ_{cr} (see Fig. 10(a)). Using the same scaling as used in Fig. 3(d) (i.e. $\phi \rightarrow r_c^2 \alpha^{0.17} \phi$), we scale the ϕ -axis. The result is shown in Fig. 10(b). We also scaled the $\psi_6 \rightarrow r_c^{-1.05} \psi_6$, which leads to a collapse of the ψ_6 value after phase separation.

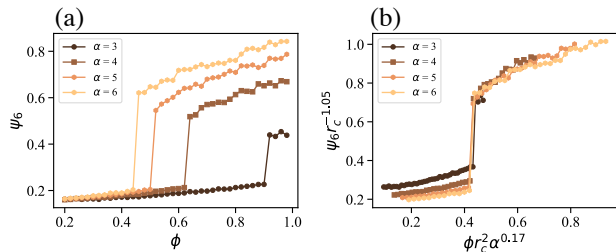


FIG. 10. (a) ψ_6 plotted as a function of ϕ at $Pe=150$ for $\alpha = 3 \rightarrow 6$. (b) Study of scaling behavior. For the phase separating cases shown in (a), the ϕ -axis is scaled as $\phi \rightarrow r_c^2 \alpha^{0.17} \phi$, while the ψ_6 is scaled as $\psi_6 \rightarrow r_c^{-1.05} \psi_6$.

In Fig. 3(d) and (e) of the maintext, we studied the dynamics of phase ordering by plotting $\psi_6(t)/\psi_6(\infty)$ as a function of time for different α . We noticed that the system exhibit a delayed transition which scales as $t \rightarrow r_c^{8.5} t$. We note two important points here: (1) The temporal scaling is applied using r_c since it is an intrinsic length-scale and can be obtained in general for any form of the potential used. We show in Fig. 11(b), that the same collapse can be obtained by using a scaling of the form $t \rightarrow \alpha^{2.8} t$. (2) The large value of the scaling exponent $\lambda = 8.5$, mainly indicates the sensitive dependence of the transition time on α ; the underlying dynamics may not be necessarily scale-free. The large exponent value may also imply that this dependence is exponential. To show this, we use an exponential scaling of the form $t \rightarrow e^{14r_c} t$ (see Fig. 11(c)) which also leads to a very good collapse of the data.

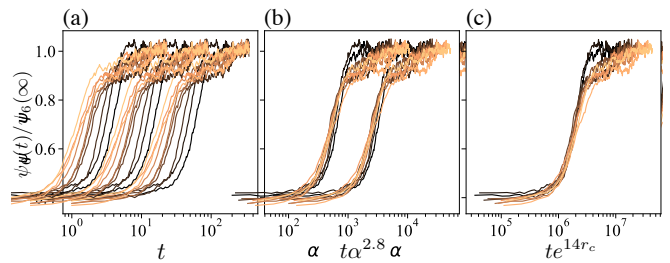


FIG. 11. (a) $\psi_6(t)/\psi_6(\infty)$ plotted as a function of time, where $\psi_6(\infty)$ is the steady-state value after the system has already phase-separated. (b) and (c) shows the temporal scaling using functions $t \rightarrow t\alpha^{2.8}$ and $t \rightarrow te^{14r_c}$ respectively, which leads to a data collapse in both the cases.

Appendix G: MSD Plots at low density

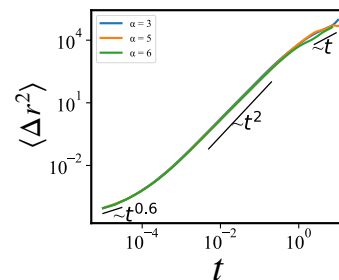


FIG. 12. Mean-square displacement for the non phase separating case at $\phi = 0.30$ and $Pe=150$ for $\alpha = 3, 5$ and 6 respectively. In all the cases we notice a crossover from sub-diffusion \rightarrow ballistic \rightarrow diffusion.

Unlike at high density, as discussed in the maintext (Fig. 4), the system exhibit ballistic transport at intermediate time scales, when the system is kept a low density ($\phi \leq 0.30$), independent of the value of for different α . This is shown in Fig. 12. In the long-time limit, the dynamics again becomes diffusive as expected. At short time scales, the dynamics is driven by thermal fluctuations but sub-diffusive due to interparticle interactions.

Appendix H: Simulation movie

Movie 1: Steady state dynamics for overlap parameter $\alpha = 3$ at $Pe=150$ and $\phi = 0.7$. Although the system does not phase separate, the dynamics is not uniform and exhibit formation of local transient clusters.

-
- [1] S. Ramaswamy, Annual Review of Condensed Matter Physics **1**, 323 (2010).
 [2] T. Vicsek and A. Zafeiris, Physics reports **517**, 71 (2012).
 [3] M. C. Marchetti, J. F. Joanny, S. Ramaswamy, T. B. Liverpool, J. Prost, M. Rao, and R. A. Simha, Rev.

- Mod. Phys. **85**, 1143 (2013).
 [4] Y. Fily and M. C. Marchetti, Phys. Rev. Lett. **108**, 235702 (2012).
 [5] G. S. Redner, M. F. Hagan, and A. Baskaran, Phys. Rev. Lett. **110**, 055701 (2013).

- [6] I. Buttinoni, J. Bialké, F. Kümmel, H. Löwen, C. Bechinger, and T. Speck, *Phys. Rev. Lett.* **110**, 238301 (2013).
- [7] M. N. van der Linden, L. C. Alexander, D. G. A. L. Aarts, and O. Dauchot, *Phys. Rev. Lett.* **123**, 098001 (2019).
- [8] A. Wysocki, R. G. Winkler, and G. Gompper, *EPL (Europhysics Letters)* **105**, 48004 (2014).
- [9] M. E. Cates and J. Tailleur, *Annual Review of Condensed Matter Physics* **6**, 219 (2015).
- [10] P. Digregorio, D. Levis, A. Suma, L. F. Cugliandolo, G. Gonnella, and I. Pagonabarraga, *Phys. Rev. Lett.* **121**, 098003 (2018).
- [11] C. B. Caporusso, P. Digregorio, D. Levis, L. F. Cugliandolo, and G. Gonnella, *Physical Review Letters* **125**, 178004 (2020).
- [12] J. Stenhammar, A. Tiribocchi, R. J. Allen, D. Marenduzzo, and M. E. Cates, *Physical review letters* **111**, 145702 (2013).
- [13] D. Levis, J. Codina, and I. Pagonabarraga, *Soft Matter* **13**, 8113 (2017).
- [14] J. U. Klamsner, S. C. Kapfer, and W. Krauth, *Nature communications* **9**, 1 (2018).
- [15] S. Paliwal and M. Dijkstra, *Physical Review Research* **2**, 012013 (2020).
- [16] S. Mandal, B. Liebchen, and H. Löwen, *Physical Review Letters* **123**, 228001 (2019).
- [17] L. Caprini, U. M. B. Marconi, and A. Puglisi, *Physical Review Letters* **124**, 078001 (2020).
- [18] S. Das and R. Chelakkot, *Soft Matter* **16**, 7250 (2020).
- [19] S. Das, S. Ghosh, and R. Chelakkot, *Physical Review E* **102**, 032619 (2020).
- [20] C. F. Lee, *New Journal of Physics* **15**, 055007 (2013).
- [21] Y. Fily, A. Baskaran, and M. F. Hagan, *Soft Matter* **10**, 5609 (2014).
- [22] J. Elgeti and G. Gompper, *EPL (Europhysics Letters)* **101**, 48003 (2013).
- [23] X.-q. Shi, G. Fausti, H. Chaté, C. Nardini, and A. Solon, *Physical Review Letters* **125**, 168001 (2020).
- [24] J. Su, H. Jiang, and Z. Hou, *New Journal of Physics* **23**, 013005 (2021).
- [25] J. Stenhammar, A. Tiribocchi, R. J. Allen, D. Marenduzzo, and M. E. Cates, *Phys. Rev. Lett.* **111**, 145702 (2013).
- [26] J. Stenhammar, D. Marenduzzo, R. J. Allen, and M. E. Cates, *Soft matter* **10**, 1489 (2014).
- [27] J. Bialké, H. Löwen, and T. Speck, *EPL (Europhysics Letters)* **103**, 30008 (2013).
- [28] T. F. F. Farage, P. Krinninger, and J. M. Brader, *Phys. Rev. E* **91**, 042310 (2015).
- [29] S. C. Kapfer and W. Krauth, *Phys. Rev. Lett.* **114**, 035702 (2015).
- [30] J. D. Weeks, D. Chandler, and H. C. Andersen, *The Journal of Chemical Physics* **54**, 5237 (1971).
- [31] M. Guo, A. F. Pegoraro, A. Mao, E. H. Zhou, P. R. Arany, Y. Han, D. T. Burnette, M. H. Jensen, K. E. Kasza, J. R. Moore, *et al.*, *Proceedings of the National Academy of Sciences* **114**, E8618 (2017).
- [32] Y. Zhou and S. T. Milner, *Soft matter* **14**, 7075 (2018).
- [33] In Eq. 4, the main α dependence comes from the terms other than C , so it is reasonable to assume C to be a constant.
- [34] M. Sanoria, R. Chelakkot, and A. Nandi, See Supplemental Movie for details.
- [35] S. C. Takatori, W. Yan, and J. F. Brady, *Physical review letters* **113**, 028103 (2014).
- [36] S. C. Takatori, W. Yan, and J. F. Brady, *Phys. Rev. Lett.* **113**, 028103 (2014).
- [37] A. P. Solon, Y. Fily, A. Baskaran, M. E. Cates, Y. Kafri, M. Kardar, and J. Tailleur, *Nature Physics* **11**, 673 (2015).
- [38] A. P. Solon, J. Stenhammar, R. Wittkowski, M. Kardar, Y. Kafri, M. E. Cates, and J. Tailleur, *Phys. Rev. Lett.* **114**, 198301 (2015).
- [39] R. G. Winkler, A. Wysocki, and G. Gompper, *Soft Matter* **11**, 6680 (2015).
- [40] S. C. Takatori and J. F. Brady, *Current opinion in colloid & interface science* **21**, 24 (2016).
- [41] A. Suma, G. Gonnella, D. Marenduzzo, and E. Orlandini, *EPL (Europhysics Letters)* **108**, 56004 (2014).
- [42] S. Mandal, B. Liebchen, and H. Löwen, *Phys. Rev. Lett.* **123**, 228001 (2019).